RESEARCH ARTICLE | MARCH 25 2011

Vector-magneto-optical generalized ellipsometry

K. Mok; N. Du; H. Schmidt

Rev. Sci. Instrum. 82, 033112 (2011)
https://doi.org/10.1063/1.3568822

Vector-magneto-optical generalized ellipsometry

K. Mok,[a] N. Du, and H. Schmidt
Institute of Ion Beam Physics and Materials Research, Helmholtz-Zentrum Dresden-Rossendorf (HZDR), P.O. Box 510119, 01314 Dresden, Germany

(Received 28 June 2010; accepted 27 February 2011; published online 25 March 2011)

We present the setup of a variable-angle vector-magneto-optical generalized ellipsometer (VMOGE) in the spectral range from 300 to 1100 nm using an octupole magnet, and demonstrate VMOGE measurements of the upper 3×4 submatrix of the Mueller matrix in a magnetic field of arbitrary orientation and magnitude up to 0.4 T at room temperature. New "field orbit" measurements can be performed without physically moving the sample, which is useful to study magnetic multilayer or nanostructure samples. A 4×4 matrix formalism is employed to model the experimental VMOGE data. Searching the best match model between experimental and calculated VMOGE data, the magneto-optical dielectric tensor $\varepsilon^{\mathrm{MO}}$ of each layer in a multilayer sample system can be determined. In this work, we assume that the nonsymmetric terms of $\varepsilon^{\mathrm{MO}}$ are induced by an external magnetic field and depend linearly on the sample magnetization. Comparison with vector magnetometer measurements can provide the anisotropic magneto-optical coupling constants Q_x, Q_y, Q_z.
 [doi:10.1063/1.3568822]

I. INTRODUCTION

For many years, the technological applications of magneto-optical (MO) materials for data storage devices have gained considerable attention. Both magnetic anisotropy and MO effects are the results of spin–orbit interactions. Anisotropy caused by extrinsic sources, e.g., by the crystal structure, grain shape, and stress also affects the nature and strength of magnetic and MO anisotropy, which is exploited in the design of most commercial magnetic materials. In general, MO response is induced by an externally applied magnetic field **H** and driven by the material magnetization **M**. For magnetically cubic, tetragonal, trigonal, hexagonal, and orthorhombic MO materials, the magnetization may be of the form $M_l = M_l(H_k), k, l = x, y, z$. Consider the MO dielectric tensor $\varepsilon^{\mathrm{MO}}$ of a given bulk sample, the magneto-optical response is described by the nonsymmetric terms $\varepsilon_{ij}^{\mathrm{MO}} = \varepsilon_{ij}^{\mathrm{MO}}(M_l)$ which are explicit functions of magnetization $M_l, l = x, y, z$.

Numerous experimental techniques are utilized for the determination of MO properties. Magneto-optical generalized ellipsometry (MOGE) has been presented as an optical tool in a theoretical work from Višňovský[1,2] and has been experimentally realized by Neuber *et al.*,[3–5] Pufall and Berger,[6] Nederpel and Martens,[7] and Halagačka *et al.*[8] So far MO ellipsometers have been combined with only one pair of solenoids[3,4,6–8] which allow to apply the magnetic field along one axis of the coordinate system. Therefore, during MOGE measurements, either the sample position or the position of the pair of solenoids has to be changed physically in order to change the orientation of the applied magnetic field with respect to the sample coordinate system. Furthermore, the system has to be calibrated after changing either of them. In this paper we describe the setup of a vector-magneto-optical generalized ellipsometer (VMOGE), which combines a generalized spectroscopic ellipsometer with an octupole magnet. This is an extended version of the MOGE setup, which is however more convenient to change the applied magnetic field orientations only by the octupole magnet while the sample remains fixed and no further calibration is required. Having the sample mounted on an automated rotation stage, VMOGE allows to perform generalized ellipsometry (GE) measurements with a magnetic field generated in 3D vector space. It also allows to perform field-free GE measurements,[9] in order to allocate optical axes and determine optical constants, which is particularly important before attempting to characterize the MO response induced by an external magnetic field. With the computer controlled octupole magnet which is built by four pairs of solenoids, mounted along the space diagonals of a cube, a magnetic field of magnitude up to 0.4 T along an arbitrary direction can be achieved at the sample position. By varying the orientation of the external magnetic field on a closed spatial loop in the 3D vector space ("field orbit") during measurements, here by means of the octupole magnet, the sample's intrinsic magnetization axes can be identified through optical responses. This is important for the analysis of MO thin films and layered nanostructure samples to study, e.g., exchange phenomena in multilayer samples, confinement, and collective magnetism. We discuss here exemplarily the investigation of a Cr_2O_3/Co/sapphire multilayer sample prepared by molecular beam epitaxy (MBE) by means of VMOGE. This sample system is chosen due to the optical isotropy and the well-known ferromagnetic properties of Co film. One can demonstrate the potential of VMOGE for identifying the magnetic uniaxial properties. Our analysis reveals that the sample magnetization follows easily any magnetic field orientation parallel to the sample surface with isotropic in-plane MO response, while nearly no magnetization perpendicular to the surface can be observed.

Using VMOGE the upper 3×4 submatrix of the Mueller matrix is measured in a magnetic field of arbitrary orientation and magnitude at room temperature, for which we determine

[a]Electronic address: kelvinmok@hzdr.de.

the MO nonsymmetric terms ε_{ij}^{MO} using a suitable model. VMOGE can also perform field-free GE measurements[9] to allocate the optical axes and to determine the optical constants of samples. To derive the MO coupling constants Q_x, Q_y, Q_z, the sample magnetization **M** is required from other experiments.

In Sec. II we discuss an approach in which the measured Mueller matrix elements can be reduced to three anisotropic magnetic-field induced (magneto-optical) dielectric function tensor elements for at least one sample constituent (a film or substrate) and also for situations where MO dielectric tensor elements for more than one sample constituent may be determined. The new VMOGE instrument and the magnetic field control are described in Sec. III A and III B, respectively. Two new measurement schemes are suggested: a "hysteresis" mode and a "field orbit" mode (Sec. III C). The "hysteresis" mode well compares with superconducting quantum interference device (SQUID) hysteresis loop measurements and is used to determine the coercive and saturation field. So far "field orbit" mode measurements can be performed with SQUID magnetometers[10] with an uniaxial sample rotation state. On the other hand, VMOGE allows for probing the MO response for arbitrary field-orbits without physically moving the sample. In Sec. III D we demonstrate that VMOGE data allow to model the MO dielectric function response of a given sample such that any angle of incidence and any field variation can be predicted. An example is shown and discussed for a multilayer sample, with one magneto-optically active sample constituent in Sec. IV. Conclusions and an outlook are given in Sec. V.

II. THEORY

A. VMOGE coordinate system

In the following we define the vector-magneto-optical generalized ellipsometer in a Cartesian coordinate system $\{x, y, z\}$ (Fig. 1). The sample surface is in the $\{x, y\}$-plane and the z axis points into the sample. The plane of incidence is the $\{x, z\}$-plane defined by the incident (**k**) and reflected (**k**′) wavevector with an oblique angle of incidence Φ_a. Referring to the direction of **H**, we label the longitudinal, transverse, and polar VMOGE configurations as (L), (T), and (P), respectively. In L-VMOGE configuration, **H** is parallel to both the sample surface and the plane of incidence ($H_x \neq 0$, $H_y = H_z = 0$). In T-VMOGE configuration, **H** is parallel to the sample surface and perpendicular to the plane of incidence ($H_y \neq 0$, $H_x = H_z = 0$). In P-VMOGE configuration, **H** is perpendicular to the sample surface ($H_z \neq 0$, $H_x = H_y = 0$). The applied magnetic field $\mathbf{H} = (H_x, H_y, H_z)$ is parameterized by magnitude H and field orientation angles φ_m, θ_m,

$$H_x = H \sin\theta_m \cos\varphi_m, \tag{1a}$$

$$H_y = H \sin\theta_m \sin\varphi_m, \tag{1b}$$

$$H_z = H \cos\theta_m, \tag{1c}$$

where the angles range within $0° < \varphi_m < 360°$ and $0° < \theta_m < 180°$. In general, reflection and transmission

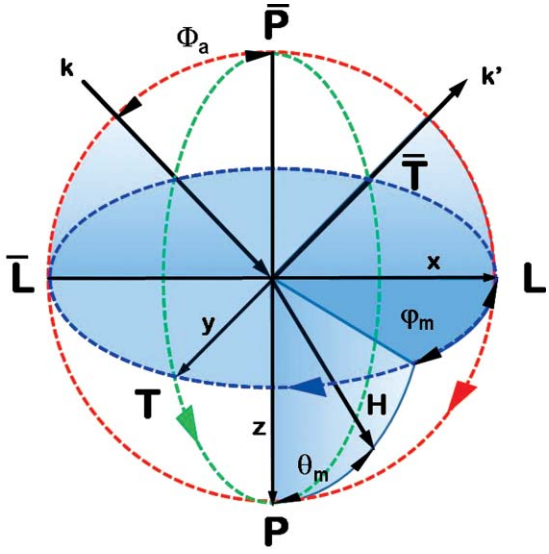

FIG. 1. (Color online) The Cartesian coordinate system $\{x, y, z\}$ of the vector-magneto-optical generalized ellipsometer (VMOGE). [definition adapted from Ref. 18] The sample surface is in the $\{x, y\}$-plane. The z axis points into the sample. The incident (**k**) and reflected (**k**′) wavevectors define the plane of incidence. The angle of incidence is Φ_a. The magnetic field $\mathbf{H} = (H_x, H_y, H_z)$ is conveniently parameterized in spherical coordinates, where H is the magnitude of field. Its orientation is given by the angles φ_m and θ_m [Eq. (1)]. The LT-, LP-, and TP-VMOGE configurations are three possible field orbit scans, defined by the orientation angles (φ_m, θ_m). LT-VMOGE ($\{x, y\}$-plane): $\theta_m = 90°$, variable φ_m; LP-VMOGE ($\{x, z\}$-plane): $\varphi_m = 0°$, variable θ_m; TP-VMOGE ($\{y, z\}$-plane): $\varphi_m = 90°$, variable θ_m.

generalized ellipsometry (GE) measurements with varying magnetic field magnitude H and arbitrarily fixed orientation (φ_m, θ_m) can be performed using VMOGE.

A special feature of the VMOGE is that GE measurements as a function of orientation angle φ_m or θ_m can be performed by sweeping **H** at $H = \text{const.}$ within a principal coordinate plane ("field orbit" mode). We denote the **H** sweeping within the $\{x, y\}$-plane as LT-VMOGE configuration, within the $\{x, z\}$-plane and $\{y, z\}$-plane as LP- and TP-VMOGE configuration, respectively. LT-, LP-, and TP-VMOGE measurements are especially important for the investigation of magnetic nanostructures deposited on flat surfaces forming macroscopically effective thin films, where the magnetic properties are governed by the spatial arrangement of the nanostructural thin film, such as for slanted nanocolumnar thin films.[11–13]

B. Mueller matrix formalism

GE determines the major axes' dielectric function tensor elements and the major axes orientations (Euler angles) for anisotropic materials. For arbitrarily anisotropic materials, the complex ratio ρ of the s- and p-polarized reflectivities depends on the polarization state of the incident light.[11,14] This concept can be represented within both the Mueller matrix as well as the Jones matrix formalism. Here we focus on the Mueller matrix presentation, which also allows for the determination of depolarization effects. The Mueller matrix M is a real valued matrix which connects the Stokes vectors of outgoing $\mathbf{S_{out}}$ and incident $\mathbf{S_{in}}$ light [Eqs. (2) and (3)],[15–17] describing the change of the electromagnetic wave properties

before and after interaction with the sample, namely

$$\mathbf{S_{out}} = M\mathbf{S_{in}}, \tag{2}$$

$$\begin{bmatrix} S_0 \\ S_1 \\ S_2 \\ S_3 \end{bmatrix}_{\text{out}} = \begin{bmatrix} M_{11} & M_{12} & M_{13} & M_{14} \\ M_{21} & M_{22} & M_{23} & M_{24} \\ M_{31} & M_{32} & M_{33} & M_{34} \\ M_{41} & M_{42} & M_{43} & M_{44} \end{bmatrix} \begin{bmatrix} S_0 \\ S_1 \\ S_2 \\ S_3 \end{bmatrix}_{\text{in}}. \tag{3}$$

The Stokes representation contains all possible polarizations of the light beam including partial polarization. The Stokes vector elements of the p- and s-polarized coordinate system are $S_0 = I_p + I_s$, $S_1 = I_p - I_s$, $S_2 = I_{45} - I_{-45}$, and $S_3 = I_{\sigma_+} - I_{\sigma_-}$, where I_p, I_s, I_{45}, I_{-45}, I_{σ_+}, and I_{σ_-} denote the intensities for the p-, $s-$, $+45^o$, -45^o, right-, and left-handed circularly polarized components of the electromagnetic wave, respectively.[11,14]

VMOGE measures the Mueller matrix of the sample and the VMOGE data need to be analyzed using the 4×4 matrix formalism,[2,9,18–20] an analytical matrix algebra based on the Berremann 4×4 formalism to calculate the Jones reflection and transmission matrix elements for arbitrarily anisotropic and homogeneously layered system.[9] The 4×4 matrix formalism also allows the evaluation of a set of 16 Mueller matrix elements in dependence of magnetic field $\mathbf{H}$ for a multilayer system. The MO dielectric tensor ε^{MO} of each layer has to be introduced for the analysis where the nonsymmetric terms $\varepsilon_{ij}^{\text{MO}}$ are assumed to be dependent of the magnetization $\mathbf{M}$ and the anisotropic complex valued MO coupling constants Q_x, Q_y, Q_z,

$$\varepsilon^{\text{MO}} = \begin{bmatrix} \varepsilon_x & -iQ_zM_z & iQ_yM_y \\ iQ_zM_z & \varepsilon_y & iQ_xM_x \\ -iQ_yM_y & -iQ_xM_x & \varepsilon_z \end{bmatrix}. \tag{4}$$

Note that Eq. (4) holds for a VMOGE setup with the same magnetic and ellipsometric Cartesian coordinate system defined in Fig. 1. In general, the magnetization is a rather complex function of magnetic field $M_l = M_l(H_k), k, l = x, y, z$, which is particularly important for monoclinic and triclinic magnetic anisotropy, as well as for layered nanostructural samples. In our work, we assumed that the magnetization of the sample is parallel to the magnetic field $\mathbf{M} \parallel \mathbf{H}$, such that $M_k = M_k(H_k), k = x, y, z$. Therefore, the L-, T, P-, LT-, LP-, and TP-VMOGE measurement modes have only access to the corresponding nonsymmetric terms of the MO dielectric tensor $\varepsilon_{ij}^{\text{MO}}$ [see Eqs. (5) and (6)]. For example, with $M_k = M_k(H_k)$, $\varepsilon_{23}^{\text{MO}} = -\varepsilon_{32}^{\text{MO}}$, $\varepsilon_{13}^{\text{MO}} = -\varepsilon_{31}^{\text{MO}}$, and $\varepsilon_{12}^{\text{MO}} = -\varepsilon_{21}^{\text{MO}}$ may be accessed from L-, T-, and P-VMOGE measurements, respectively.

One should be clear that the VMOGE technique determines the magneto-optically active nonsymmetric terms $\varepsilon_{ij}^{\text{MO}}$ of the sample, by fitting the experimental and calculated Mueller matrix data using the best match model. It cannot measure Q_x, Q_y, Q_z and $\mathbf{M}$ independently. In order to obtain the MO coupling constants Q_x, Q_y, Q_z, additional experiment is needed to measure the magnetization of each layer in a multilayer sample, e.g., using a SQUID. The MO coupling constants Q_x, Q_y, Q_z are simply constants of magnetic field in the magnetization-dependent nonsymmetric terms $\varepsilon_{ij}^{\text{MO}}$. The motivation of assuming the nonsymmetric terms $\varepsilon_{ij}^{\text{MO}} \propto Q_k M_k, k = x, y, z$ is to obtain field-independent Q_x, Q_y, Q_z. Furthermore, this assumption allows to distinguish the anisotropy of the MO coupling constants Q_x, Q_y, Q_z and the magnetization $\mathbf{M}$.

As an example, if an external magnetic field H_x is applied, namely performing a L-VMOGE measurement and if one may assume that $M_y = M_z = 0$ for $H_y = H_z = 0$, the ε^{MO} describing the L-VMOGE mode simplifies to

$$\varepsilon^{\text{MO}} = \begin{bmatrix} \varepsilon_x & 0 & 0 \\ 0 & \varepsilon_y & iQ_xM_x(H_x) \\ 0 & -iQ_xM_x(H_x) & \varepsilon_z \end{bmatrix}. \tag{5}$$

Only a pair of the ε^{MO} nonsymmetric term $\varepsilon_{23}^{\text{MO}} = -\varepsilon_{32}^{\text{MO}} = iQ_xM_x(H_x)$ is nonzero and can be determined. Then the $M_x(H_x)$ has to be measured separately such that Q_x can be obtained.

In case of the VMOGE field orbit measurements (LP-, TP-, LT-VMOGE), two pairs of the nonsymmetric terms can be accessed. For example, the ε^{MO} of LT-VMOGE mode is given by

$$\varepsilon^{\text{MO}} = \begin{bmatrix} \varepsilon_x & 0 & iQ_yM_y(H_y) \\ 0 & \varepsilon_y & iQ_xM_x(H_x) \\ -iQ_yM_y(H_y) & -iQ_xM_x(H_x) & \varepsilon_z \end{bmatrix}. \tag{6}$$

Note that the Q_x, Q_y, Q_z presented in this paper might be defined differently from other research work.[3,4,6,7,21–30] Therefore, it is more convenient to compare values of $\varepsilon_{ij}^{\text{MO}}$, for example of $\varepsilon_{32}^{\text{MO}} = -\varepsilon_{23}^{\text{MO}}$ from L-VMOGE experiment [Fig. 7(a)].

III. EXPERIMENTAL SETUP AND DATA ANALYSIS

A. VMOGE setup

The octupole magnet and the sample holder stage have been designed and constructed in close collaboration between Anderberg & Modéer Accelerator AB (AMACC), Sweden, and J.A. Woollam Co., Inc., USA. The magnet stage is mounted to a commercial rotating analyzer ellipsometer VASE®. Figure 2 shows schematic drawings of the side and top view of the octupole magnet. Four pairs of solenoids are fixed along the space diagonals of a cube within the magnet frame. The spatial arrangement of the solenoids can be seen in Figs. 2(a) and 2(b). Four bipolar power supplies (Kepco, Inc.) are used for controlling currents I_1, I_2, I_3, and I_4 [Fig. 2(c)] through the four pairs of solenoids of the octupole magnet. The cylindrical cores of the solenoids are made from nonmagnetic rods (AMACC), and leave an approximate free sample space between the individual core pairs of $10 \times 10 \times 10$ mm^3 at the center of the quadrupole arrangement. Samples with a total thickness up to 1 mm and a surface area up to 10×10 mm^2 can be mounted on a brass-made sample holder, and can be vertically inserted from the top plate into the center of the four solenoids pair axes [Fig. 2(b)]. This design allows to perform VMOGE measurements both in reflection and transmission mode. For the sample alignment, the

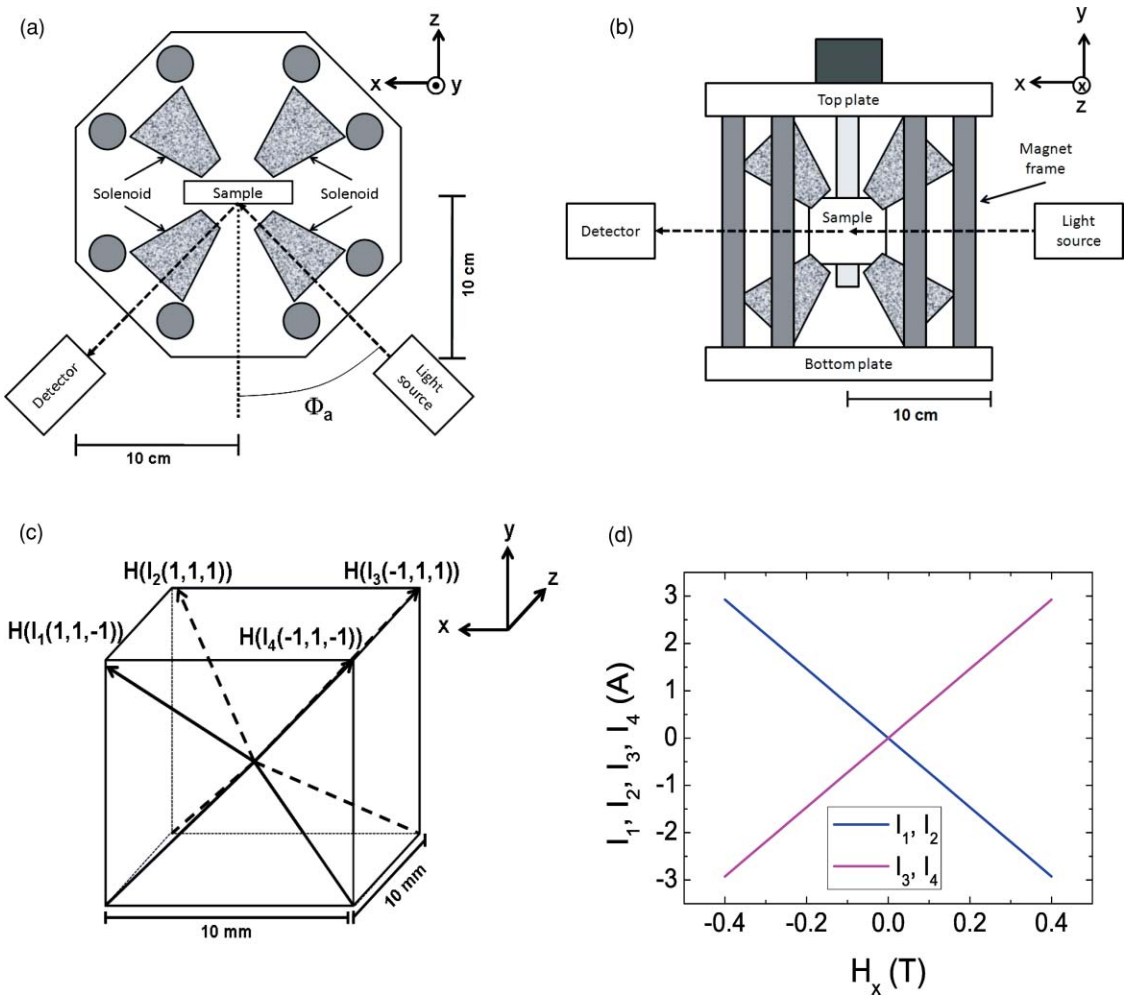

FIG. 2. (Color online) Top (a) and side (b) views of the octupole magnet. Four pairs of solenoids are built along the space diagonals of a cube in the magnet. The magnet frame is formed by a top and a bottom plate together with four pairs of vertical nonmagnetic rods located near the solenoids. (c) indicates the four currents (I_1, I_2, I_3, I_4) through the four solenoid pairs for the generation of the magnetic field $\mathbf{H}$ as the vector sum of magnetic fields $H(I_1)$, $H(I_2)$, $H(I_3)$, and $H(I_4)$ oriented along normalized coordinates $\vec{e_1} = (1, 1, -1)$, $\vec{e_2} = (1, 1, 1)$, $\vec{e_3} = (-1, 1, 1)$, and $\vec{e_4} = (-1, 1, -1)$, i.e., along the cubic space diagonals. The represented magnetic Cartesian coordinate is the same as the ellipsometric Cartesian coordinate system defined in Fig. 1. (d) shows the relation between the currents (I_1, I_2, I_3, I_4) and the magnetic field $\mathbf{H} = (H_x, 0, 0)$ obtained from calibration.

implemented software of VASE is used, and the mechanical support of the octupole magnet has sufficient degrees of freedom to ensure that the sample surface is placed perpendicular to the probe beam. The vertical sample holder can be translated along or rotated about the y axis, while the magnet support can be translated along the z axis and its horizontal plane is able to be tilted. A wide range of angles of incidence can be accommodated, leaving two unaccessible angle ranges from $\Phi_a = 22.5^\circ$ to 37.3° and from $\Phi_a = 52.7^\circ$ to 67.5° where the probe beam is blocked by the magnet support frame (see Fig. 10). The probing area of the ellipsometric measurement on the sample surface at $\Phi_a = 45^\circ$ is $\sim 3 \times 3$ mm^2, and typically extends to $\sim$8 mm in the plane of incidence at $\Phi_a = 70^\circ$. The actual probe size area depends on the collimating system of the ellipsometer and range from 1×1 to 2×2 mm^2 for normal incidence. The homogeneity of the magnetic field strength at $H = \pm 0.4$ T amounts to $\sim$3.5% over a $3 \times 3 \times 3$ mm^3 large sample space.

Using the presented VMOGE setup, we determine 11 Mueller matrix elements from the upper 3×4 submatrix of the Mueller matrix, normalized to the Mueller matrix element M_{11}. The rotating analyzer ellipsometer used here contains only one compensator, thus the fourth row of the Mueller matrix is not measured.[19,31] However, it does not impair the accessibility of the normalized Jones matrix elements, except for its absolute phase, which can be obtained only by including an additional compensator.[32] Hofmann *et al.* have reported several papers about Mueller matrix ellipsometry using a similar rotating analyzer ellipsometer.[33–35]

B. Field control

A Hall effect teslameter was used to determine the magnetic field strength and direction along three axes as a function of currents (I_1, I_2, I_3, I_4). The relation between the currents (I_1, I_2, I_3, I_4) and the magnetic field (H_x, H_y, H_z) is sufficiently linear up to a current of 3 A and is described by Eqs. (7),

$$\begin{aligned} -I_1\vec{e_1} - I_2\vec{e_2} + I_3\vec{e_3} + I_4\vec{e_4} &= -4\alpha H_x, \\ I_1\vec{e_1} + I_2\vec{e_2} + I_3\vec{e_3} + I_4\vec{e_2} &= 4\alpha H_y, \\ I_1\vec{e_1} - I_2\vec{e_2} - I_3\vec{e_3} + I_4\vec{e_2} &= -4\alpha H_z, \end{aligned} \tag{7}$$

where $\vec{e}_1 = (1, 1, -1)$, $\vec{e}_2 = (1, 1, 1)$, $\vec{e}_3 = (-1, 1, 1)$, $\vec{e}_4 = (-1, 1, -1)$ are the space diagonal unit vectors [Fig. 2(c)], and $\alpha = 7.31$ A/T depends on the magnet design. By rearranging the above equations, we obtain

$$\begin{aligned} I_1\vec{e}_1 &= 2\alpha H_y - 2\alpha H_z - I_4\vec{e}_4, \\ I_2\vec{e}_2 &= 2\alpha H_x + 2\alpha H_z + I_4\vec{e}_4, \\ I_3\vec{e}_3 &= -2\alpha H_x + 2\alpha H_y - I_4\vec{e}_4. \end{aligned} \tag{8}$$

The set of Eqs. (8) is overdetermined, i.e., it has no unique solution. To obtain a unique solution of the current set (I_1, I_2, I_3, I_4), the smallest possible sum of all currents for a given magnetic field vector **H** has to be taken as the fourth operation condition. The obtained solution is called the "minimum norm solution." Using the minimum norm solution for the four currents (I_1, I_2, I_3, I_4), it is ensured that the variation of the magnitude and direction of the magnetic field is continuous. Figure 2(d) shows the relation between the currents (I_1, I_2, I_3, I_4) and the magnetic field $\mathbf{H} = (H_x, 0, 0)$ obtained from calibration.

C. Data acquisition

The VMOGE setup is fully controlled by a computer program. Two different VMOGE measurement modes may be performed:

- Hysteresis measurement: by applying the magnetic field **H** along an arbitrary, fixed axis with variable field magnitude and orientation through inversion of the field direction by the origin of the octupole magnet (L-, T-, P-VMOGE),
- Field orbit measurement: by applying the magnetic field **H** along an arbitrary, closed spatial loop with variable magnetic field orientation (φ_m, θ_m) and constant field magnitude (LT-, LP-, TP-VMOGE).

Figure 1 indicates the $\{x, y\}$-, $\{x, z\}$-, and $\{y, z\}$-field orbit loops with constant magnetic field magnitude, namely the LT- ($\{x, y\}$-plane), LP- ($\{x, z\}$-plane), and TP-VMOGE ($\{y, z\}$-plane) configurations, respectively. The spatial field orbit is defined by the field orientation angles φ_m and θ_m.

The VMOGE data acquisition process of hysteresis and field orbit mode is shown in Fig. 3. The system is calibrated using the regression calibration method for a rotating analyzer ellipsometer described in Ref. 36. A wavelength within the range from 300 to 1100 nm and the angle of incidence are set. Note that for certain angles of incidence the probe beam is blocked by the octupole magnet support frame. The measurement mode, i.e., hysteresis (L-, T-, P-VMOGE) or field orbit (LT-, LP-, TP-VMOGE) measurement has to be chosen. For controlling the octupole magnet, magnetic field parameters, such as maximum field $H_{k,\max}$, field step ΔH_k, and orbital angle step $\Delta\varphi_m$ or $\Delta\theta_m$ are set with respect to the chosen measurement mode. The number of measurement points which depends on the measurement parameter increment has to be calculated. The Mueller matrix elements as a function of magnetic field orientation and magnitude are measured by the ellipsometer. For the used VASE, the experimental precision of the measured Mueller matrix elements amounts to 10^{-4}.

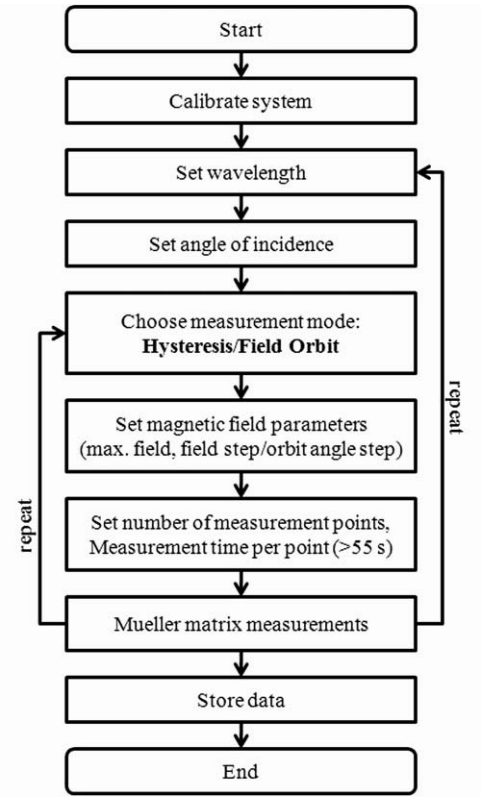

FIG. 3. Flowchart of the VMOGE data acquisition of hysteresis and field orbit measurement modes. The Mueller matrix elements are probed as a function of the magnetic field magnitude and orientation.

D. Data analysis

Figure 4 shows a flowchart of the VMOGE data analysis. In general, for an optically anisotropic sample system, field-free GE is required to determine the principal-axis dielectric function $(\varepsilon_x, \varepsilon_y, \varepsilon_z)$ of $\varepsilon^{\mathrm{MO}}$ and the thickness d of each layer. Ellipsometric data analysis using numerical regression technique and by comparing calculated data to measured data yields $(\varepsilon_x, \varepsilon_y, \varepsilon_z)$ and d of each layer. If the investigated multilayer sample contains thick and highly absorbing layers, GE is in general not sufficient to determine the layer thickness, instead other techniques would be required for such purpose. However, for metallic and optically isotropic multilayer stacks with thickness below 40 nm, spectroscopic ellipsometry measurements and data analysis is an established method for film thickness and optical constant determination. Note that the stack thickness of metallic multilayers in giant magnetoresistance or tunnel magnetoresistance devices is typically smaller than 40 nm.[37]

Derived from $\varepsilon^{\mathrm{MO}}$, Mueller matrix elements as functions of magnetic field, wavelength, and angle of incidence can be calculated via the 4×4 matrix formalism and compared with the experimental Mueller matrix data. Fitting the nonsymmetric terms $\varepsilon_{ij}^{\mathrm{MO}}$ with the calculated and experimental data to search for the best match model of $\varepsilon^{\mathrm{MO}}$.

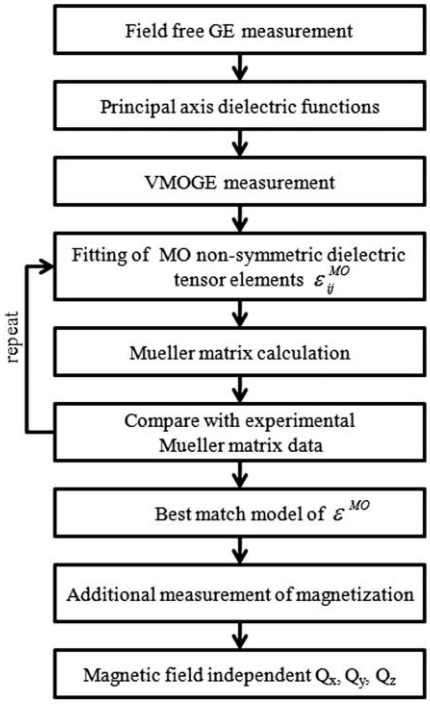

FIG. 4. Flowchart of the analysis of VMOGE data. Best match model between calculated and experimental data is obtained from the MO dielectric tensor $\varepsilon^{\mathrm{MO}}$ analysis. Having additional measurement of magnetization **M**, the magnetic field independent MO coupling constants Q_x, Q_y, Q_z can be determined.

Finally, only if additional information on the magnetization properties of the sample can be obtained, the nonsymmetric terms $\varepsilon_{ij}^{\mathrm{MO}}$ can be separated into the wavelength dependent, magnetic field independent MO coupling constants Q_x, Q_y, Q_z, and the wavelength independent, magnetic field dependent magnetization $M_k(H_l)$, with $k, l = x, y, z$. By a comparison with the experimental determined $M_k(H_l)$, the anisotropic MO coupling constants Q_x, Q_y, Q_z can be obtained. With such information, the magnetic anisotropy of $M_k(H_l)$ may be identified. So far, the vector Preisach model has been used to extract the time-dependent nonlinear relation between magnetic field and magnetization of anisotropic samples from a series of magnetization measurements and to easily follow the magnetization evolution in anisotropic samples.[38]

IV. RESULTS AND DISCUSSION

As an example, we investigated an optically isotropic Cr_2O_3/Co/sapphire multilayer sample with VMOGE, in order to reveal the uniaxial magnetic anisotropy of the Co layer. The MBE technique was used for the growth of a Co thin film on c-plane sapphire substrate, followed by a Cr layer on top. The Cr layer immediately oxidizes outside the MBE chamber, forming a thin Cr_2O_3 film preventing further oxidation of the underlying Co film.

Spectroscopic ellipsometry (SE) measurements under zero magnetic field condition is important to determine the optical properties of the Cr_2O_3/Co/sapphire multilayer sample. Actually, the sapphire substrate is an uniaxial material.[39]

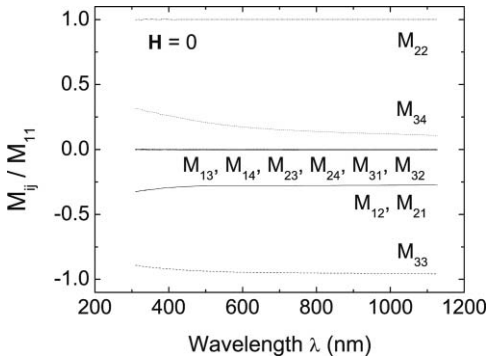

FIG. 5. Zero-field normalized Mueller matrix data from the Cr_2O_3/Co/sapphire multilayer sample as a function of wavelength at 45° angle of incidence.

However, treating the substrate isotropic, i.e., $\varepsilon_x = \varepsilon_y = \varepsilon_z = \varepsilon$, it is sufficient to model the VMOGE data here. The determined film thicknesses are 8 and 2 nm for the Co and Cr_2O_3 thin films, respectively. Furthermore, field-free Mueller matrix measurements were performed on the sample over a spectral range from 300 to 1100 nm at 45° angle of incidence (Fig. 5). Eleven Mueller matrix elements M_{ij}, normalized by the total intensity, i.e., M_{11} were measured. M_{13}, M_{14}, M_{23}, M_{24}, M_{31}, and M_{32} are zero, while M_{12}, M_{21}, M_{22}, M_{33}, and M_{34} are finite and depend on the wavelength. The results are typical for an isotropic sample.

By applying an external magnetic field H_x, i.e., performing L-VMOGE measurement, a MO response of the sample is induced and the Mueller matrix elements M_{13}, M_{14}, M_{23}, M_{24}, M_{31}, and M_{32} become finite. Figure 6(a) shows the experimental and calculated data of three Mueller matrix element differences $\Delta M_{ij} = M_{ij}(-H_x) - M_{ij}(H_x)$ normalized to M_{11} at 45° angle of incidence and external magnetic field $H_x = \pm 90$ mT. Note that Co thin film is saturated under the magnetic field of $H_x = \pm 90$ mT. ΔM_{13}, ΔM_{24}, and ΔM_{31} are presented as they depend strongly on magnetic field and are detectable by means of VMOGE system. For the magnetic field H_y applied along the y axis (T-VMOGE), the largest MO response is shown in ΔM_{12}, ΔM_{21}, ΔM_{33}, and ΔM_{34} [Fig. 6(b)].

Finding the best matching between the experimental and calculated data, the nonsymmetric terms $\varepsilon_{32}^{\mathrm{MO}}$ and $\varepsilon_{31}^{\mathrm{MO}}$ are determined by the L-VMOGE and T-VMOGE data, respectively (Fig. 7). $\varepsilon_{32}^{\mathrm{MO}} = \varepsilon_{31}^{\mathrm{MO}}$ revealed that the Co film is magneto-optically in-plane isotropic. Optically, the sample might be not perfectly isotropic, hence the misfit of experimental and calculated ΔM_{33} occurred. However, this would not influence the determined $\varepsilon_{31}^{\mathrm{MO}}$. Schmidt *et al.*[12] reported the $\varepsilon_{12}^{\mathrm{MO}}$ extracted from polar MOGE measurement data probed on a reference sample with a 60 nm thick Co film, where a much larger field of 1.8 T had to be applied in order to saturate the out-of plane magnetization of the investigated uniaxial anisotropic magnetic Co film. The sign, order of magnitude, and wavelength dependence of the extracted nonsymmetric MO dielectric tensor terms $\varepsilon_{32}^{\mathrm{MO}}$ and $\varepsilon_{31}^{\mathrm{MO}}$ for L-VMOGE and T-VMOGE, respectively, well agree with the reported $\varepsilon_{12}^{\mathrm{MO}}$.[12]

We assumed that $\varepsilon_{ij}^{\mathrm{MO}}$ is a product of the magnetic field independent MO coupling constant Q_k and the

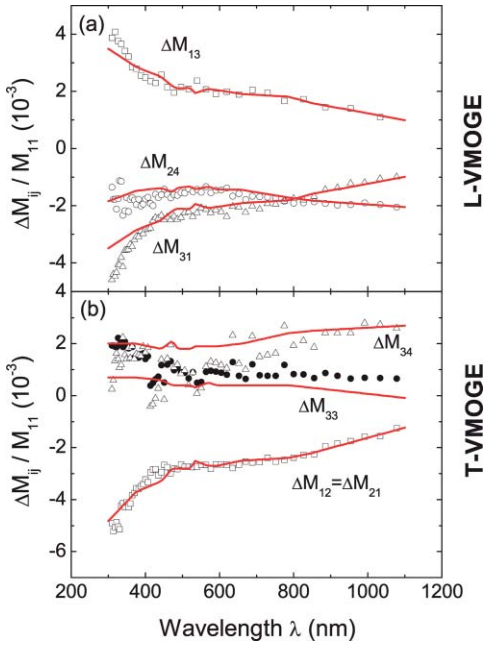

FIG. 6. (Color online) Experimental (symbols) and calculated (line) Mueller matrix element difference $\Delta M_{ij} = M_{ij}(-H_{x,y}) - M_{ij}(H_{x,y})$ normalized to M_{11} at 45° angle of incidence and external magnetic field: (a) $H_x = \pm$ 90 mT (L-VMOGE) and (b) $H_y = \pm$ 90 mT (T-VMOGE) for the Cr_2O_3/Co/sapphire multilayer sample.

magnetization M_k [Eqs. (4) and (5)]. Hence, the sample magnetization was measured using a SQUID magnetometer (Quantum Design MPMS) on a sample piece with the Co film mass of 1.78 μg. The Co film mass is derived from the SE determined film thickness 8 nm and the density of Co. SQUID results (Fig. 8) reveal

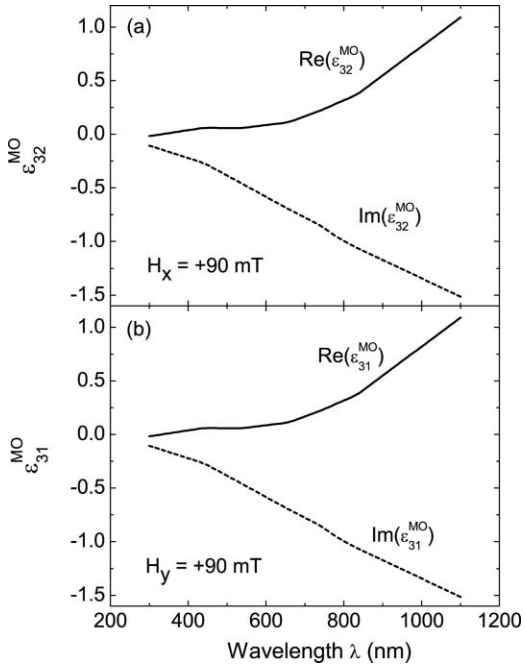

FIG. 7. The modeled nonsymmetric MO dielectric tensor terms (a) ε_{32}^{MO} from L-VMOGE ($H_x = +90$ mT) and (b) ε_{31}^{MO} from T-VMOGE ($H_y = +90$ mT) for Co film in the Cr_2O_3/Co/sapphire multilayer sample.

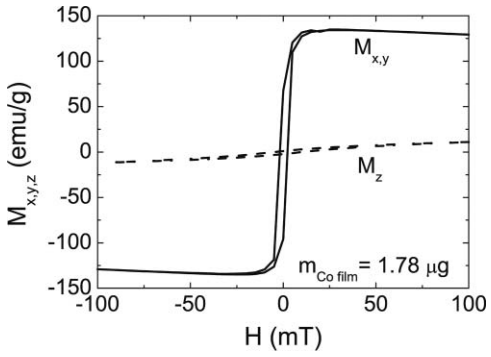

FIG. 8. Mass normalized layer magnetization **M** of the Co thin film probed in-plane ($M_{x,y}$) and out-of-plane (M_z). The Co film mass of 1.78 μg is derived from the SE determined film thickness and the density of Co.

that the Co thin film is ferromagnetic with the easy and hard axes of magnetization lying in-plane and out-of-plane, respectively. The in-plane magnetization is isotropic $M_x = M_y$, saturated above 20 mT and amounts to about 130 emu/g. The out-of plane magnetization typically reaches its saturation value at around 800 mT.[40] Below a magnetic field strength of 100 mT, the magnetization of the antiferromagnetic Cr_2O_3 top layer[41,42] and the diamagnetic sapphire substrate is much smaller than the magnetization of the ferromagnetic Co thin film and may be neglected. For simplicity, we assumed only the ε_{ij}^{MO} of the Co layer of the Cr_2O_3/Co/sapphire multilayer sample to be nonzero.

Figure 9 shows L-, LT-, and LP-VMOGE data recorded on the sample with 442 nm wavelength at 45° angle of incidence. The 442 nm wavelength is chosen since it is often used as an excitation source for magnetic wide band gap semiconductors in laser-based MO measurement setups.[43] Hysteresis behavior of the normalized M_{13} and M_{24} from L-VMOGE measurement is directly proportional to the corresponding nonsymmetric terms ε_{23}^{MO} and ε_{32}^{MO} of ε^{MO}, which are linearly proportional to M_x [Eq. (5)]. A complex magnetic field independent MO coupling constant Q_x of Co film is obtained by factoring out M_x from ε_{32}^{MO}, which amounts to Q_x =(0.00193 + i0.00044) g/emu at a wavelength of 442 nm. Also the analysis of LT-VMOGE data using the Eq. (6) revealed that the MO coupling constants (Q_x, Q_y, Q_z) of our Co film is sufficiently in-plane isotropic, i.e., $Q_x = Q_y$ and $Q_z = 0$ are obtained.

LP-VMOGE measurement revealed that M_{13} and M_{24} are step functions of θ_m and evidenced that the z axis of Co film is the magnetic hard axis. Abrupt changes occur at $\theta_m = 180°$. This effect is due to the alignment of magnetic moments along the x axis, i.e., the easy axis during the rotation of θ_m. For the calculation of Mueller matrix elements, the LP-VMOGE dielectric tensor for the sample studied here can be represented by using sign functions

$$\varepsilon^{MO} = \begin{bmatrix} \varepsilon & 0 & 0 \\ 0 & \varepsilon & iQ_xM_xsign(H_x) \\ 0 & -iQ_xM_xsign(H_x) & \varepsilon \end{bmatrix}, \quad (9)$$

where $H_x = H\sin\theta_m\cos\varphi_m = H\sin\theta_m$ [Eq. (1)] with $\varphi_m = 0°$ in LP-VMOGE mode, and it is assumed that M_x is saturated, i.e., independent of **H**. Here, the magnetization effect

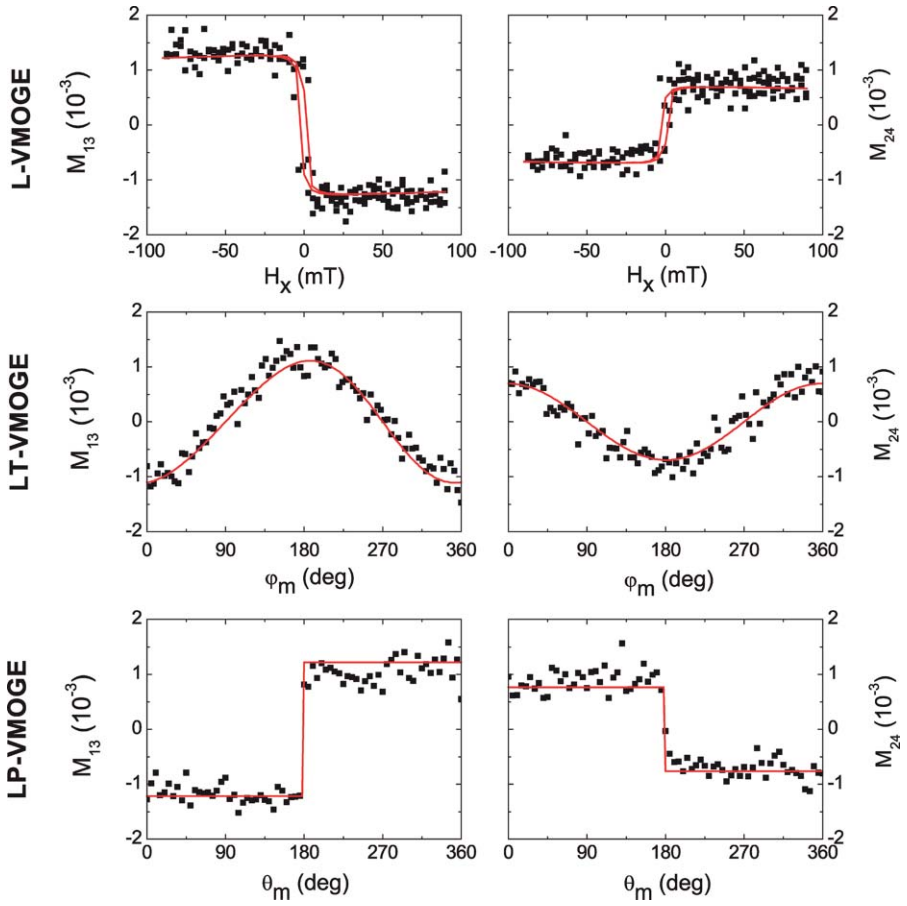

FIG. 9. (Color online) L-, LT-, and LP-VMOGE measurements performed on the Cr_2O_3/Co/sapphire multilayer sample with 442 nm wavelength at 45° angle of incidence. The normalized Mueller matrix elements M_{13} and M_{24} were measured (symbols) simultaneously from each of the measurements and the modeling (line) results in a unique complex MO coupling constant $Q_x(\lambda = 442\ \text{nm}) = (0.00193 + i0.00044)$ g/emu. In LP-VMOGE measurement, steplike functions of M_{13} and M_{24} were detected, abrupt changes occur at $\theta_m = 180°$.

along the hard axis is neglected, i.e., only the magnetization along x axis contributes to the tensor.

L-VMOGE measurements at different angles of incidence Φ_a have also been performed. Measuring the normalized Mueller matrix elements M_{13} and M_{24} under a magnetic field of $H_x = +90$ mT with 442 nm wavelength, we recognize that M_{13} and M_{24} strongly depend on Φ_a (Fig. 10). According to the best match model calculated data, the maxima of M_{13} and M_{24} occur at around $\Phi_a = 58°$. The choice of the angle of incidence is important to optimize the magnetic field dependent Mueller matrix elements. This representation reveals the predictive ability of the presented VMOGE setup and underlines the importance to choose Φ_a in the range from 45° to 75°.

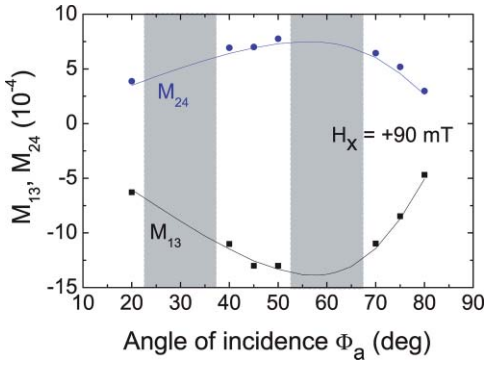

FIG. 10. (Color online) Measured (symbol) and calculated (line) Mueller matrix elements M_{13} and M_{24} as a function of the angle of incidence Φ_a with 442 nm wavelength at $H_x = +90$ mT. The shaded areas indicate the two Φ_a ranges where the ellipsometer probe beam is blocked by the frame construction of the octupole magnet [Figs. 2(a) and 2(b)].

Using the VMOGE setup, magneto-optical Kerr effect (MOKE) investigations may also be performed by measuring the Fresnels' reflection coefficients r_{pp}, r_{ss}, r_{ps}, and r_{sp} being defined as the ratio between the p- and s-components of incident and reflected electromagnetic waves. Having the Fresnels' reflection coefficients, the Kerr rotation θ_K and ellipticity η_K can be evaluated as follows:[44]

$$\theta_K + i\eta_K = -r_{ps}/r_{pp}. \tag{10}$$

Figure 11 shows the experimental and calculated longitudinal ($H_x = +90$ mT) and transverse ($H_y = +90$ mT) MOKE data recorded at 45° angle of incidence on the Cr_2O_3/Co/sapphire sample. The Kerr rotation θ_K and ellipticity η_K are calculated by assuming the identical ε_{32}^{MO} and ε_{31}^{MO} (Fig. 7), which are previously obtained from the L-VMOGE and T-VMOGE data, respectively. The longitudinal MOKE measurement data slightly deviates from the predicted data and the measured Kerr ellipticity η_K has relatively

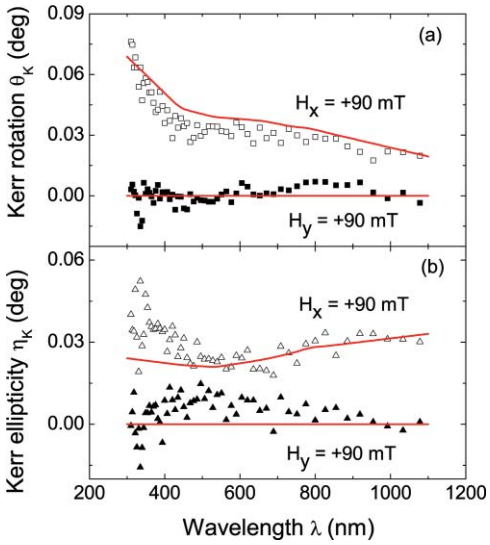

FIG. 11. (Color online) Experimental (symbols) and calculated (line) longitudinal ($H_x = +90$ mT) and transverse ($H_y = +90$ mT) MOKE data at 45° angle of incidence of the Cr_2O_3/Co/sapphire multilayer sample in the spectral range from 300 nm to 1100 nm. (a) θ_K and (b) η_K of longitudinal and transverse MOKE are calculated using the modeled ε_{32}^{MO} and ε_{31}^{MO} in Fig. 7, respectively.

larger noise. For the transverse MOKE measurements, θ_K and η_K should vanish, as this has been proven by Postava *et al.* theoretically.[45] However, we recorded nonzero data from the sample. This could be explained if the sample is slightly magnetized longitudinally due to the misalignment of the applied magnetic field direction. Thus, we claim that the Mueller matrix ellipsometry is a more powerful method for the modeling of ε^{MO} and Q_x, Q_y, Q_z, since the effect of different magnetic field orientations reflects on different sets of Mueller matrix elements (Fig. 6). Besides, consider the noise of MOKE data, VMOGE system is more suitable for Mueller matrix measurement. Figure 12 shows the θ_K and η_K as a function of the angle of incidence Φ_a, measured with 442 nm wavelength at $H_x = +90$ mT. The error of the Kerr ellipticity $\eta_K(\Phi_a)$ is much larger than $\theta_K(\Phi_a)$, which can also be seen in Fig. 11.

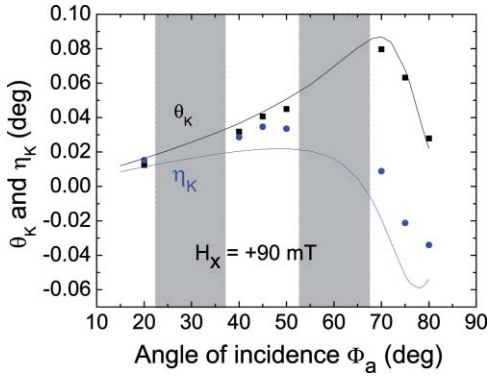

FIG. 12. (Color online) Measured (symbol) and calculated (line) Kerr rotation θ_K and η_K as a function of the angle of incidence Φ_a with 442 nm wavelength at $H_x = +90$ mT. The shaded areas indicate the two Φ_a ranges where the ellipsometer probe beam is blocked by the frame construction of the octupole magnet [Figs. 2(a) and 2(b)].

V. CONCLUSIONS AND OUTLOOK

MO properties of materials which have been studied so far by MOKE setup at certain fixed angle of incidence, can also be investigated by VMOGE technique at an oblique angle of incidence. We have demonstrated that the VMOGE technique allows to perform field-free generalized ellipsometry measurements as well as field-dependent Mueller matrix and Kerr angle measurements of magnetic anisotropic multilayer samples. A new "field-orbit" measurement features the VMOGE and it is especially important for the investigation of magnetic anisotropic material, e.g., magnetic nanostructural thin films. If additional information on the magnetization properties of the sample can be obtained, e.g., from SQUID measurements, the nonsymmetric terms of ε^{MO} can be separated into the magnetic-field independent functions Q_k and the magnetic-field dependent functions $M_k(H_k)$. For a given multilayer sample, the measured Mueller matrix elements at fixed wavelength and magnetic field depend on the angle of incidence Φ_a. VMOGE allows to choose a predicted optimal angle of incidence Φ_a for optimizing the measured VMOGE data. As an example, we discussed here a ferromagnetic Cr_2O_3/Co/sapphire multilayer sample. We propose VMOGE as an ideal tool to study artificially fabricated magnetic anisotropic systems, e.g., slanted nanocolumnar thin films,[11–13] or Ni and Co nanowires[40] with a very strong magnetic anisotropy. By improving the accuracy and speed of VMOGE systems, this new technique can potentially replace MOKE for the study of MO anisotropy in multilayer samples. Furthermore, a redesign of the magnet frame may help to extend the range of possible angles of incidence. In the near future, new spectroscopic ellipsometers with further developed performance regarding accuracy and speed will possibly replace laser-based magneto-optical setups performed at ambient conditions.

ACKNOWLEDGMENTS

The authors would like to acknowledge financial support from the Bundesministerium für Bildung und Forschung (FKZ 13N10144). We also thank M. O. Liedke from HZDR for the sample preparation; S. Zhou from HZDR for the SQUID measurements; C. Bunce from HZDR, T. Wagner from LOT-Oriel Co., B. Anderberg from AMACC, and G. Cooney and C. Herzinger from Woollam Co. for technical support; M. Schubert, T. Hofmann, and D. Schmidt from University Nebraska-Lincoln for the very fruitful discussions.

[1] Š. Višňovský, Czech. J. Phys., Sect. B **36**, 625 (1986).
[2] Š. Višňovský, K. Postava, and T. Yamaguchi, Czech. J. Phys. **51**, 917 (2001).
[3] G. Neuber, R. Rauer, J. Kunze, T. Korn, C. Pels, G. Meier, U. Merkt, J. Bäckström, and M. Rübhausen, Appl. Phys. Lett. **83**, 4509 (2003).
[4] G. Neuber, R. Rauer, J. Kunze, J. Bäckström, and M. Rübhausen, Thin Solid Films **455–456**, 39 (2004).
[5] R. Rauer, G. Neuber, J. Kunze, J. Bäckström, and M. Rübhausen, Rev. Sci. Instrum. **76**, 023910 (2005).
[6] A. Berger and M. R. Pufall, Appl. Phys. Lett. **71**, 965 (1997).
[7] P. Q. J. Nederpel and J. W. D. Martens, Rev. Sci. Instrum. **56**, 687 (1985).
[8] L. Halagačka, K. Postava, M. Foldyna, and J. Piscarontora, Phys. Status Solidi A **205**, 752 (2008).
[9] M. Schubert, Thin Solid Films **313–314**, 323 (1998).

[10]D. M. Pajerowski and M. W. Meisel, J. Phys.: Conf. Ser. **150**, 012034 (2009).
[11]D. Schmidt, A. C. Kjerstad, T. Hofmann, R. Skomski, E. Schubert, and M. Schubert, J. Appl. Phys. **105**, 113508 (2009).
[12]D. Schmidt, T. Hofmann, C. M. Herzinger, E. Schubert, and M. Schubert, Appl. Phys. Lett. **96**, 091906 (2010).
[13]J. Gospodyn and J. Sit, Opt. Mater. **29**, 318 (2006).
[14]T. Hofmann, U. Schade, C. M. Herzinger, P. Esquinazi, and M. Schubert, Rev. Sci. Instrum. **77**, 063902 (2006).
[15]A. Laskarakis, S. Logothetidis, E. Pavlopoulou, and M. Gioti, Thin Solid Films **455–456**, 43 (2004).
[16]J. N. Hilfiker, C. M. Herzinger, T. Wagner, A. Marino, G. Delgais, and G. Abbate, Thin Solid Films **455–456**, 591 (2004).
[17]D. A. Ramsey and K. C. Ludema, Rev. Sci. Instrum. **65**, 2874 (1994).
[18]M. Schubert, *Infrared Ellipsometry on Semiconductor Layer Structures: Phonons, Plasmons, and Polaritons* (Springer, Berlin, 2005).
[19]H. Fujiwara, *Spectroscopic Ellipsometry, Principle and Applications* (Wiley, Japan, 2007).
[20]M. Schubert, Phys. Rev. B **53**, 4265 (1996).
[21]M. Buchmeier, R. Schreiber, D. E. Bürgler, and C. M. Schneider, Phys. Rev. B **79**, 064402 (2009).
[22]X. Gao, M. J. DeVries, D. W. Thompson, and J. A. Woollam, J. Appl. Phys. **88**, 2775 (2000).
[23]C.-Y. You and S.-C. Shin, Thin Solid Films **493**, 226 (2005).
[24]R. Atkinson, S. Pahirathan, I. Salter, C. Tatnall, J. Lodder, Q. Meng, and P. Grundy, J. Magn. Magn. Mater. **162**, 131 (1996).
[25]R. Atkinson, W. Hendren, I. Salter, and M. Walker, J. Magn. Magn. Mat. **130**, 442 (1994).
[26]M. Foldyna, K. Postava, D. Ciprian, and J. Pistora, J. Magn. Magn. Mat. **290–291**, 120 (2005).
[27]Z. Q. Qiu and S. D. Bader, Rev. Sci. Instrum. **71**, 1243 (2000).
[28]Z. J. Yang and M. R. Scheinfein, J. Appl. Phys. **74**, 6810 (1993).
[29]Y. Ino, R. Shimano, Y. Svirko, and M. Kuwata-Gonokami, Phys. Rev. B **70**, 155101 (2004).
[30]X. Gao, D. W. Glenn, S. Heckens, D. W. Thompson, and J. A. Woollam, J. Appl. Phys. **82**, 4525 (1997).
[31]G. E. Jellison and F. A. Modine, Appl. Opt. **36**, 8190 (1997).
[32]M. Schubert, T. Hofmann, and C. M. Herzinger, J. Opt. Soc. Am. A **20**, 347 (2003).
[33]T. Hofmann, C. M. Herzinger, C. Krahmer, K. Streubel, and M. Schubert, Phys. Status Solidi A **205**, 779 (2008).
[34]T. Hofmann, V. Darakchieva, B. Monemar, H. Lu, W. J. Schaff, and M. Schubert, J. Electron Mater. **37**, 611 (2008).
[35]T. Hofmann, C. V. Middendorff, V. Gottschalch, and M. Schubert, Phys. Status Solidi C **5**, 1386 (2008).
[36]B. Johs, Thin Solid Films **234**, 395 (1993).
[37]P. Grünberg, R. Schreiber, Y. Pang, M. B. Brodsky, and H. Sowers, Phys. Rev. Lett. **57**, 2442 (1986).
[38]G. Bertotti, J. Appl. Phys. **69**, 4608 (1991).
[39]H. Yao and C. H. Yan, J. Appl. Phys. **85**, 6717 (1999).
[40]K. Ounadjela, R. Ferré, L. Louail, J. M. George, J. L. Maurice, L. Piraux, and S. Dubois, J. Appl. Phys. **81**, 5455 (1997).
[41]S. A. Makhlouf, J. Magn. Magn. Mat. **272–276**, 1530 (2004).
[42]D. Vollath, D. V. Szabó, and J. O. Willis, Mater. Lett. **29**, 271 (1996).
[43]H. Falk, W. Heimbrodt, P. Klar, J. Hübner, M. Oestreich, and W. W. Rühle, Phys. Status Solidi B **229**, 781 (2002).
[44]W. A. McGahan, P. He, L.-Y. Chen, S. Bonafede, J. A. Woollam, F. Sequeda, T. McDaniel, and H. Do, J. Appl. Phys. **69**, 4568 (1991).
[45]K. Postava, O. Životský, J. Pištora, and T. Yamaguchi, Thin Solid Films **455–456**, 615 (2004).